Topological excitation of singly hydrated hydroxide complex in confined sub-nanospace for bright color emission and heterogeneous catalysis

Xiao-Dan Hu,[1] Tai-Qun Yang,[1] Bing-Qian Shan,[1] Bo Peng,[1] Kun Zhang[1,2,3]*

[1] Shanghai Key Laboratory of Green Chemistry and Chemical Processes, Laboratory of Interface and Water Science, College of Chemistry and Molecular Engineering, East China Normal University, Shanghai 200062, China;

[2] Laboratoire de chimie, Ecole Normale Supérieure de Lyon, Institut de Chimie de Lyon, Université de Lyon, 46 Allée d'italie, 69364 Lyon cedex 07, France;

[3] Shandong Provincial Key Laboratory of Chemical Energy Storage and Novel Cell Technology, School of Chemistry and Chemical Engineering, Liaocheng University, Liaocheng, 252059, Shandong, P. R. China.

* Correspondence: kzhang@chem.ecnu.edu.cn (K.Z.)

Abstract

Conventional photoluminescence (PL) emission of individual chromophores follows the classical local excitation based on the Franck-Condon model. More and more evidences showed that small molecules even with non-conjugated structure can emit strong bright colors, e.g., water molecules at confined interface.[1-5] However, the elucidation on the structure and the physicochemical origin of water emitters remains elusive. Here, using thermally activated zeolites with well-defined molecular-scale cavities as a model confined space, combined with a panel of ex- and in-situ experimental techniques, we confirm that the structural water molecules in form of singly hydrated hydroxide complex are real emitter centers, and its colors and quantum efficiency strongly depend on the H-Bond interactions in the subnano-sized microenvironments. Furthermore, the ultra-fast femtosecond transient absorption (fs-TA) kinetic measurement unveils an unusual multichannel nonradiative mechanism dominated by proton tunneling, suggesting a unique feature of topological excitation (TE) due to many-body quantum localization (MBQL).[6-9] Our findings of multiple sets of dynamic interface states at confined interface not only answer the physical origin of water emitters, but also provide new insights into the dynamical microscopic pathway to heterogeneous catalysis.

Introduction

Intrinsically free water is generally considered a colorless liquid. However, more and more experimental results evidenced that water molecules could emit bright and tunable colors when confined at nanoscale interface.[1-5] Obviously, this abnormal PL phenomenon is intuitively hard to accept by the local excitation theory since there is no conjugated structure in water compared with classical fluorescent molecules. By a careful examination for the sporadic publications, this peculiar PL system, not only limited to inorganic water molecules, but also included some non-conjugated organic molecules (amino acids) or protective organic ligands,[10-17] which shows several very

common and unique features in the steady and transient spectra, such as multiple sets of coupled absorption and emission bands with ultra-large Stokes shift, extremely susceptible to the structural inhomogeneity, local environments and external stimulus (pH, solvent, temperature and ion, etc.), and unusual multichannel excitation energy and electron transfer behavior. These observations indicate the formation of exotic metastable excited states at nanoscale interface underlying unusual small molecule−surface interaction with strong many electrons correlations, which is a reminiscent of direct observation of dynamical switching between chemisorption state and physisorption state to adsorption in heterogeneous catalysis.[18,19]

In this report, using Ag^+ exchanged Linde Type A (LTA) zeolites as model confined system, we provide solid evidence that the emitter center of PL zeolites was singly hydrated hydroxyl complex adsorbed onto Ag^+ in the zeolite frameworks with a definite stoichiometric ratio of Ag to hydroxide and/or water (1:1), instead of Ag nanoclusters (NCs) confined in the subnano-channels of zeolites. Since LTA zeolites even not processed by Ag^+ exchange also showed an identical PL emission behavior to that of Ag exchanged zeolites. By following the decay kinetics of excited states using femtosecond transient absorption (fs-TA) technique, combined with the steady absorption and PL spectra, we demonstrated that, the production of multiple sets of coupled absorption and emission bands was attributed to the topological excitation due to MBQL effect.

Results and Discussions

Identification of singly hydrated hydroxyl complex as real emitter center for PL emission.

The Ag-exchanged LTA (Ag@LTA) zeolites were synthesized by thermally activation as previously reported method.[3,20-24] Scanning electron microscopy (SEM), High-resolution transmission (HRTEM) and X-ray diffraction (XRD) revealed that Ag cations were successfully exchanged into zeolite frameworks by K^+ substitution of 4A (Fig. 1a and Fig. S1), and we didn't find Ag presented in nanoclusters (NCs) or nanoparticles (NPs), which precludes the possibility of PL origin to the NCs centers. Very importantly note that, the features of PL of Ag@LTA are strongly dependent on the thermal activation in both preparation and measurement (Fig. 1c, 1d and Fig. 2a), the pH value (Fig. 1e) and the nature of solvent (Fig. 2b-e). With an increase of thermal activation temperature from RT to 500 ^oC, a new broad emission band peaking at ca. 530 nm emerged, and its intensity gradually increased maximum at 450 ^oC, and then decreased. Concomitantly, the same evolution of the corresponding excitation bands with separated peaks at 270, 310 and 367 nm was observed (Fig. 1c). Very interestingly, we found that, after thermal activation of Ag exchanged LTA, the pH value of Ag@LTA in water solution was basic and was gradually increased to 9.55 at 450 ^oC (Fig. 1d). However, when further rising

up temperature, pH was significantly increased, accompanying a drastic decrease of PL emission (Fig. 1c), suggesting a pivotal role of structural water or hydroxyl in the frameworks of zeolite to tune the PL. This was confirmed by thermalgravimetric (TG) analysis where the decomposition of structural water molecules and/or hydroxyl groups at 300 ^{o}C was observed (Fig. 1f).

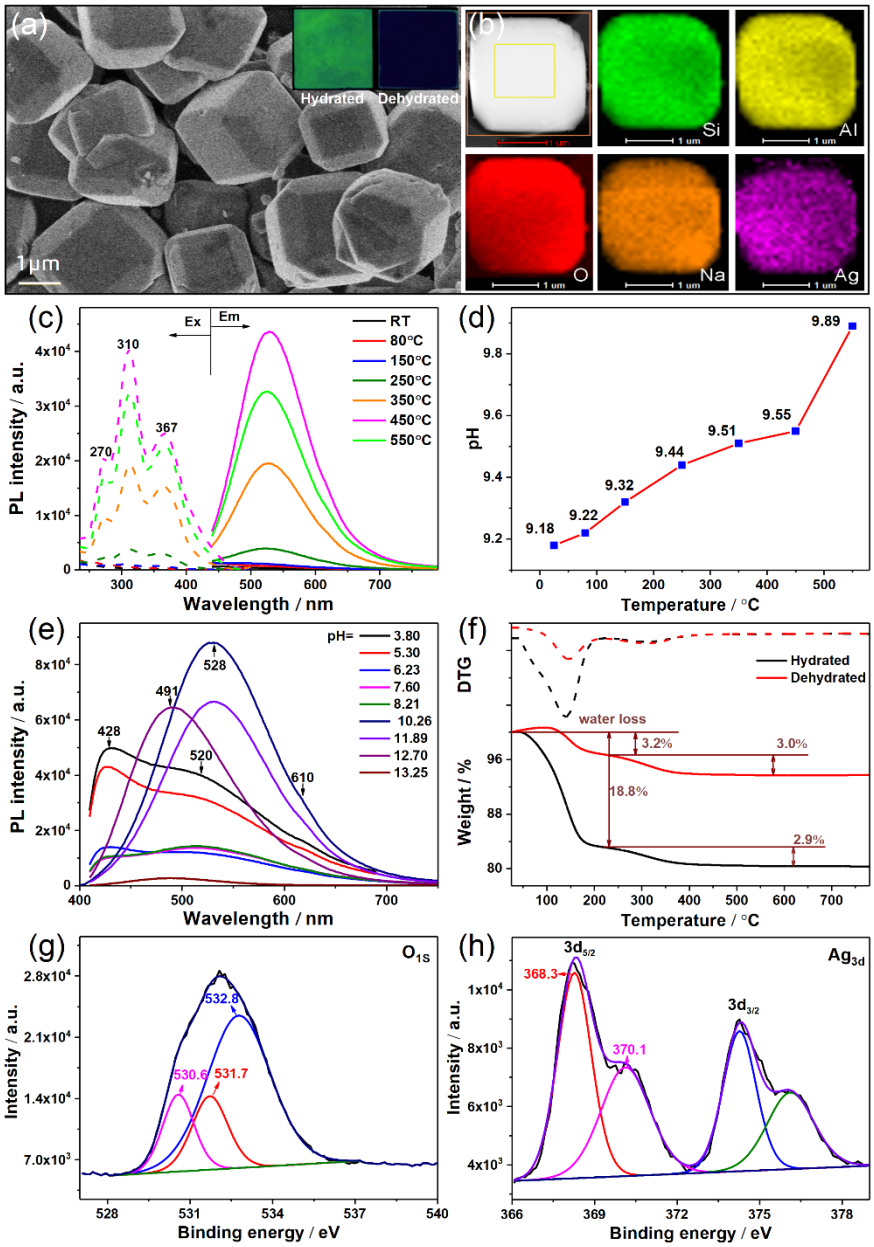

Figure 1. (a) Scanning electron microscopy (SEM) images of Ag@LTA-450 ^{o}C. The insert shows the corresponding digital photos in hydrated and dehydrated state under UV light. (b) High-resolution HAADF-STEM (white) images of Ag@LTA-450 ^{o}C and corresponding STEM EDX mapping images of Si (green), Al (yellow), O (red), Na (orange) and Ag (purple), respectively. Excitation and emission spectra of Ag@LTA annealed at different temperatures (c) and corresponding pH value of Ag@LTA dispersed in water (d). (e) Emission spectra of Ag@LTA-450 ^{o}C solution at different pH condition. (f) TG-DTG analysis of Ag@LTA-450 ^{o}C in hydrated and dehydrated state. (g) O_{1s} and Ag_{3d} XPS spectra Ag@LTA-450 ^{o}C.

The designed diagnostic experiment of pH changes on the effect of PL of thermally activated Ag@LTA at 450 ^{o}C further proved our hypothesis. With the decrease of pH, PL emission was blue-shifted from 530 nm to 430 nm, but three main broad emission bands peaking at 430 nm, 530 nm and 610 nm can be easily distinguished (Fig. 1e). A close inspection on excitation spectrum showed that, a new excitation band peaking at 270 nm appeared and intensified with the pH decrease, accompanying the weakening of band at ca. 260 nm, but other two bands at ca. 300 and ca. 360 nm were almost not changed (Fig. S2). Because thermally activated mother zeolites exhibit the weak alkalinity with pH of 9.55, the addition of acid will neutralize the structural hydroxyl groups with Lewis basic character, probably leading to the formation of weak coordinated water molecules to Ag cations, which answers the disappearing of excitation band at 270 nm assigned to ligand to metal charge transfer (LMCT) of OH^- to Ag^+, but strengthening of excitation band at ca. 300 nm due to LMCT of water to Ag^+. This also answered why oxygen and silver atoms of Ag@LTA on XPS have two groups of paired binding energy (BE) with equivalent molar ratio (Fig.1, g and h, Table S1). Obviously, acid-base neutralization did not result in the complete quenching of the fluorescence of zeolites, only the change of the PL intensity of different luminescent centers.

Another remarkable PL feature of Ag@LTA is its environmental sensitivity, especially water molecules with weak H-Bonds surrounding the luminescent centers. Reversible emission evolution of thermally activated Ag@LTA upon dehydration/hydration in vacuum/water vapor was observed (Fig. 2a and Fig. 3a). Indeed, the simple dehydration process only quenched green PL excited at 365 nm. However when dehydrated sample was irradiated at much short wavelength of even 254 nm, very strong red PL emission was observed with very large Stokes shift of 350 nm, suggesting a completely new PL emission mechanism. Similar phenomenon was observed, but its PL origin was attributed to the quantum confinement effect of Ag NCs.[23,24] It should be mentioned that, the simple dehydration only removes the physically adsorbed water molecules, instead of structural water and hydroxyl groups due to the strong chemisorption with covalent bonding. Solvent dependent PL behavior further proved this point (Fig. 2b-e).

As dehydration process, with the increase of f_{DMSO} (f_{DMSO} = volume ratio of DMSO to water), PL emission was noncontinuously shifted from 525 to 605 nm (Fig. 2, b and d), suggesting the simultaneous presence of two emitter centers. Since DMSO is bad solvent for water, the water molecules surrounding structural water and hydroxyl groups by weak H-bond interactions could be readily extracted. The results of excitation spectrum confirmed this point: when f_{DMSO} is larger than 85%, the excitation band centered at 290 nm is equally branched into two bands at 278 and 300 nm, which presumably corresponds to LMCT of $OH^-\rightarrow Ag^+$ and $H_2O\rightarrow Ag^+$, respectively (Fig. 2c). But it is importantly noted that, when the green emitter center was dominated emission, three main excitation bands peaking at 315, 370 and 405 nm were not

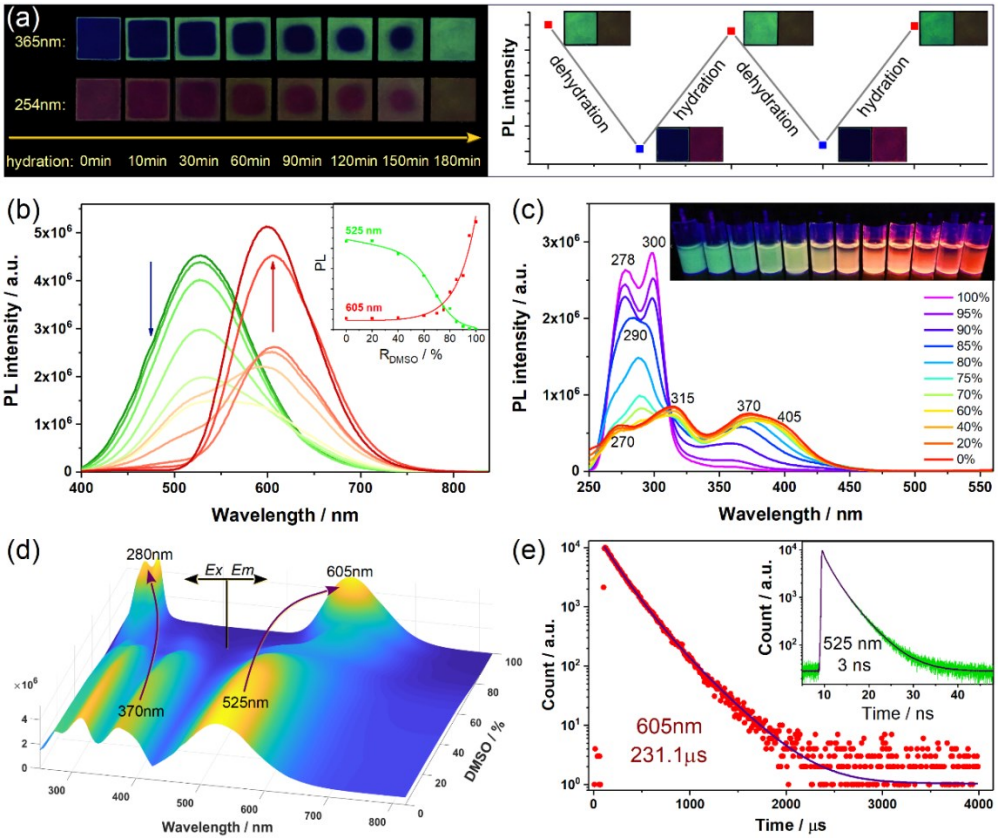

Figure 2. (a) Left, digital photos of LTA-AgNCs under UV light during the hydration process. Right, evolution of fluorescence emission intensity (at 525 nm) of Ag@LTA-450 ^{o}C with alternating cycles of dehydration and hydration process and corresponding digital photos under UV light (365 nm). Photoluminescence (b) and UV−vis absorption spectra (c) of Ag@LTA-450 ^{o}C in the varied volume fraction of DMSO in the mixed solvent (f_d = V_{DMSO} / $V_{DMSO+water}$). Photoluminescence was excited at 370 nm. (d) Contour representation of the excitation and emission data with varied R_d for Ag@LTA-450 ^{o}C. (e) Time-resolved luminescence decay profiles of Ag@LTA-450 ^{o}C in water (green) and DMSO (red) solution.

unambiguously assigned. It is well known that, proton transfer or shuttling in the confined namespace relying on H-bond networks constructed by surrounding water molecules, significantly influences the coordination interaction between ligand and metal, in particular for hydroxide or hydroxyl groups with strong Lewis base characteristic. This probably answers that Ag@LTA in DMSO solution exhibits unprecedented ultra-long quantum lifetime up to ca. 231.1 μs, by four orders of magnitude increase to Ag@LTA in water solution in 3 ns (Fig. 2e), since the proton transfer dramatically slows down due to breaking of H-bond networks when surrounding water molecules were removed.[25] The isotope effect of heavy water further proves that the rate of proton transfer has an important effect on fluorescence emission. When heavy water was introduced, the intensity of both PL and excitation bands was significantly increased with red-shifts of ca. 5 wavenumbers (Fig. 3b), since the diffusion of D^+ is slower than H^+ in the H-bond networks.

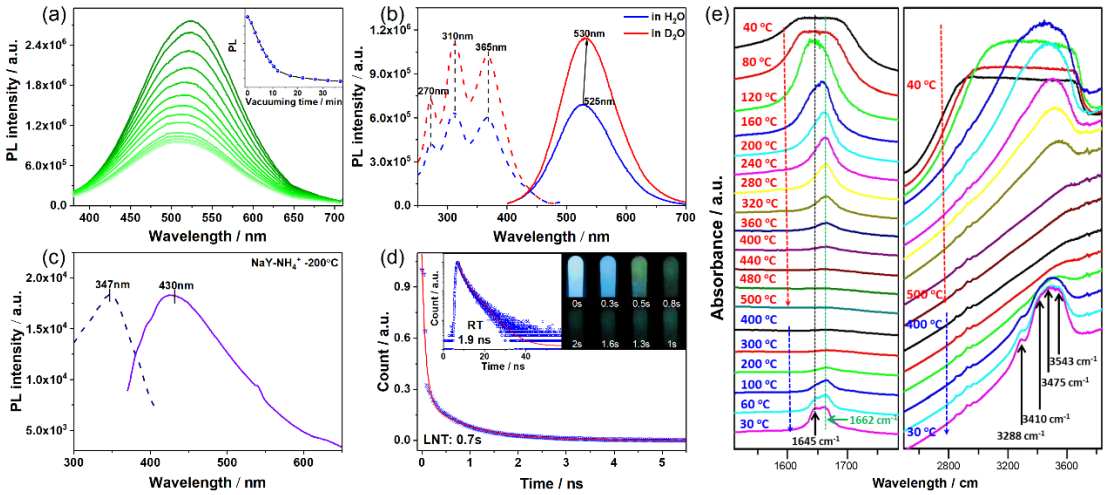

Figure 3. (a) PL decrement of hydrated Ag@LTA-450 °C with increasing time of vacuumizing. Inset shows the corresponding PL intensity attenuation (at 525 nm) during the dehydration process. (b) Comparison of emission properties of Ag@LTA-450 °C in H_2O and D_2O. (c) Excitation (dashed line) and emission spectra (solid line) of NH_4^+-Y-type zeolite annealed at 200 °C. (d) Time-resolved luminescence decay profiles of NH_4^+-Y-type zeolite at room temperature (RT) and liquid nitrogen temperature (LNT). Inset shows the naked eye visible long afterglow emission at LNT. (e) In situ DRIFTS spectrum of Ag@LTA-450 °C during a programmed heating and cooling process.

These important controlled experiments disclosed that the characteristic of this multi-colorful emission is strongly associated with the coordinating hydroxide (or hydroxyl) and water molecules to the Ag ions, which is clear evidence for that the efficient emission from Ag activated zeolites may not originate from the quantum confinement effect of Ag NCs. This conclusion was supported by the fact that, even without any metal ions, the ammonium exchanged NaY (NH_4^+@Y) after thermal activation at 200 °C emitted strong blue fluorescence at ca. 370 nm with a unique feature of classical chromophore molecules (Fig. 3c). Notably emphasized that, to our surprises, the fluorescence and excitation spectra of NH_4^+@Y are almost the same as those of Ag^+@LTA at low pH value (Fig. 1 e), implying the same emitter center, innocent to Ag ions or NCs. More surprisingly, when the PL of thermally activated NH_4^+@Y was measured at liquid nitrogen temperature (LNT), it first show blue colors, and then displayed the delayed green fluorescence emission at nanosecond scale (Fig. 3d), suggesting a nature of multi-channel radiation decay of same luminous center. Note that, the quantum lifetime of several seconds is just in the scale of the breaking and making of O-H bonds in water molecules, in well-agreement with the results recorded by EPR and STEM observations.[18,25] In-situ diffuse reflectance fourier transform infrared spectroscopy (DRIFTS) at varied temperatures provided the direct evidence for the reversible formation of structure water molecules (Fig. 3e): with the increase of measurement temperature, the intensity of bending mode of OH in water, corresponding to structural water molecules and hydroxyl groups at 1645 and 1662 cm^{-1}, respectively, was gradually decreased and almost

disappeared at 500 ^{o}C. Similar evolution trend in higher wavenumber region was also observed to the OH stretching mode of water.[4] This answers that, Ag@LTA lost the principal PL emission when its thermally activated temperature is above 500^{o}C due to the removal of structure water molecules (Fig. 1c). When temperature was cooled down to RT under trace of water atmosphere, structural hydroxyl groups at 1662 cm^{-1} was first produced in very short times, however the formation of structural water at 1645 cm^{-1} needed longer times in second scale due to the proton shuttling and subsequent reaction, and finally when the equilibrium was arrived, the coupled water-hydroxyl pairs in precise molar ration of 1:1 were recovered (Fig. 3 e). It is importantly noted that, thermally activated NH_4^+@LTA didn't show the reversible change of hydroxyl to water (Fig. S4), probably due to acid-base neutralization occurring in extremely fast time involving the fast proton mobility of Bronsted acid active sites in the framework of zeolites. The temperature-dependent reaction equation for the reversal formation of singly hydrous hydroxyl complex in the confined sub-nano space of zeolite can be written as such:

$$2Ag^{+} + 2H_2O \rightarrow AgOH^{*} + AgH_2O^{*} + H^{*}$$

$$AgOH^{*} + AgH_2O^{*} + H^{*} \rightarrow AgOH^{*} + AgOH^{*} + 2H^{*}$$

$$AgOH^{*} + AgOH^{*} + 2H^{*} \rightarrow Ag_2O + H_2O + 2H^{*}$$

Taken all together, we definitively confirmed that, the emitter center of thermally activated zeolites is coupled water molecules in the form of singly hydrous hydroxyl complexes, and that Ag ion, protons and even incompletely exchanged alkali metal ions in the inorganic frameworks just play an adsorbed site for the immobilization of emitter center. Obviously, the overlapping of p orbitals of coupled or paired O atoms though space interaction formed unusual transient excited states,[26,27] resulting in abnormal PL emissions with multiple sets of absorption and excitation bands.

Nature of excited states of singly hydrous hydroxide complex in confined sub-nanospaces.

To follow the dynamics of excited state of coupled water pair in the confined nanocavity, the femtosecond time-resolved ultra-fast transient absorption (TA) spectra were performed. However, due to the high scattering of Ag@LTA zeolites in solution, the signal collecting with high signal to noise is not available. Fortunately, Ag NCs synthesized using PAA as protective template showed the identical PL emission behavior to Ag@LTA in water and DMSO solution,[10,11] such as multiple set of excitation and emission bands, suggesting a common nature for PL origin (Fig. 4a, 4b and Fig. S5). The distinctive difference is slight red-shifts of emission wavelengths with varied life times, probably due to the delicate change of confined microenvironments. Thus, the

non-scattering Ag NCs in water and DMSO solution is an ideal model to study the dynamic decay of excited states by TA.

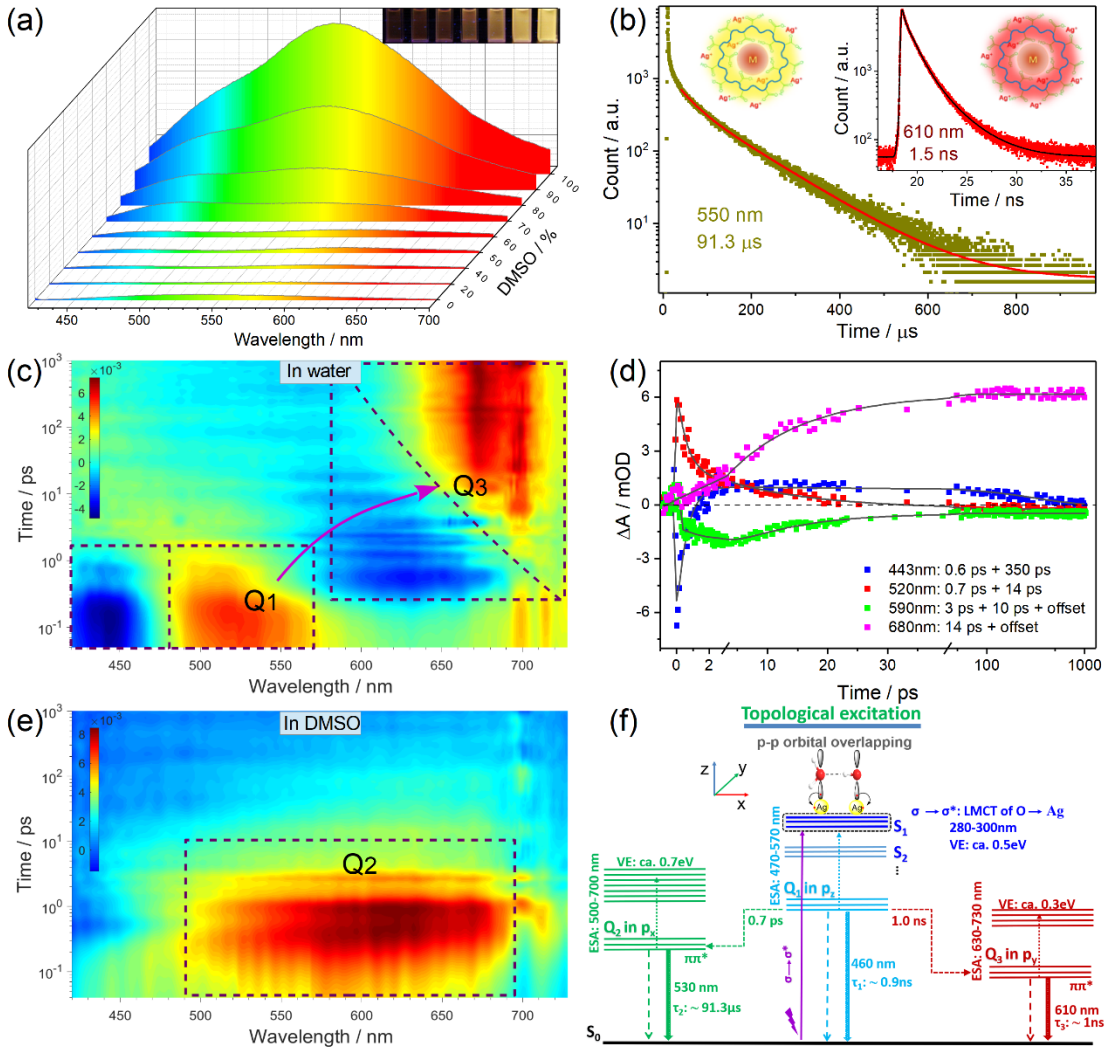

Figure 4. (a) Photoluminescence spectra of PAA-Ag NCs in the varied volume fraction of DMSO in the mixed solvent (f_d = V_{DMSO} / $V_{DMSO+water}$). Photoluminescence was excited at 365 nm. (b) Time-resolved luminescence decay profiles of PAA-Ag NCs in water (610 nm) and DMSO (550 nm) solution. Contour representation of the multidimensional time-resolved absorption data for PAA-AgNCs in water (c) and DMSO (e) solution with an excitation of 365 nm. (d) Selected decay traces and corresponding fitting of PAA-AgNCs in water solution; the fitting results are summarized in Table S4. (f) Energy levels, relaxation pathway of WCs under different solvent conditions (Q_n means the multiple quantum states, which is produced by many-body nuclear quantum effect).

Figure 4c and 4e depict 3D fs-TA spectra of Ag NCs after excitation at 365 nm in water and DMSO solution, respectively. When Ag NCs are dispersed into the water, two set of positive and negative signals peaking at ~ 520, 443 and ~ 680, 590 nm with distinct decay properties are observed, indicating the presence of two transient species or states (denoted as Q1 and Q3). The negative signals are originated from the stimulated emissions (SE) of two steady fluorescent emissions peaking at ~ 460 and ~ 610 nm in the nearly

same region (Fig.4 a, Fig. S5 and Table S4). We interestingly find that the decays of these positive and negative signals are strongly correlated in the ultra-fast time scales by multiexponential fitting of time profiles (Fig. 4 d and Table S5): the build-up time (0.6 ps) of SE at ~ 443 nm completely mirrors the decay (0.7 ps) of excited state absorptions (ESA) at ~ 520 nm at the very early stage after the photoexcitation, providing clear evidence for removal of the excitonic species (Q1) or state population by state transfer; similar decay of ESA at ~ 680 nm and SE at ~ 590 nm is observed (Fig. 4d and Table S5), but with long-lasting time constant (~ 14 ps), suggesting a main charge transfer (CT) channel to PL state at ~ 590 nm (Q1→Q2).

In DMSO solution, the main ESA (Q2) take place at ~630 nm, featuring the continuous and structureless absorption in the all visible range, but ESA at 520 and 680 nm are still observed (Fig. 4 e). Apart of this delicate changes, the spectral and temporal evolution of the spectra of Ag NCs in the first picosecond is nearly identical in water (Table S5), indicating that these transient species and state have common features and physical origins. Further global analysis of the decay profiles of Ag NCs at all wavelengths (Fig. S6, S7 and Table S5) demonstrate a complex dynamic requiring a description by multiexponentials containing at least three components with time constants in the early sub-picosecond (τ_1 = ~ 0.5 ps), a dozen picoseconds (τ_2 = ~ 10 ps), and about several nanoseconds (τ_3 > 1.0 ns, the longest delay time accessible by our measurement) time scale. The fractional contribution ($\boldsymbol{\alpha}$%) of each component (Table S5) is very sensitive to solvent type, in parallel to the properties of optical absorption and PL emission (Fig. 4 a and 4b, and Fig. S5), e.g., ultra-long lifetimes in second time scale of thermally activated NH_4^+@Y at LNT (Fig. 3c and 3d). The similar complex dynamic appearing to be yet another frequently reported feature of electronically excited DNAs,[14-16] including a few previously studied GQs structures. Cation effect on the electronic excited states of guanine nanostructures studied by time-resolved fluorescence spectroscopy,[28-30] which is attributed to the interface electronic coupling, while completely neglecting the role of structural water molecules as emitter centers.

The fs-TA and steady absorption and emission spectra put together suggests a scenario of deactivation (Fig. 4 f) involving the energy delocalized excitation producing an ensemble of states (Q_n) with mutually different polarizations that decay via multiple channels. The observed multiple set of transient species or states (Q_n) are concurrently produced, and the main optical absorption and emission are extremely susceptible to delicate change of microenvironments surrounding at the emitter center. In water solution, the Q_1 and Q_3 are dominating species. Even though these two species could produced independently in extremely fast sub-picosecond time scale, the population of Q_3 state is mostly achieved by fast excitation charge transfer (ECT) from Q_1 state. The ultra-fast ECT feature probably answers the broad and non-structure excited state absorptions of Q_2 in DMSO solution. This

clearly answered that, Ag NCs in DMSO solution emit brightest emission (~530 nm) with much longer life times (91 μs).

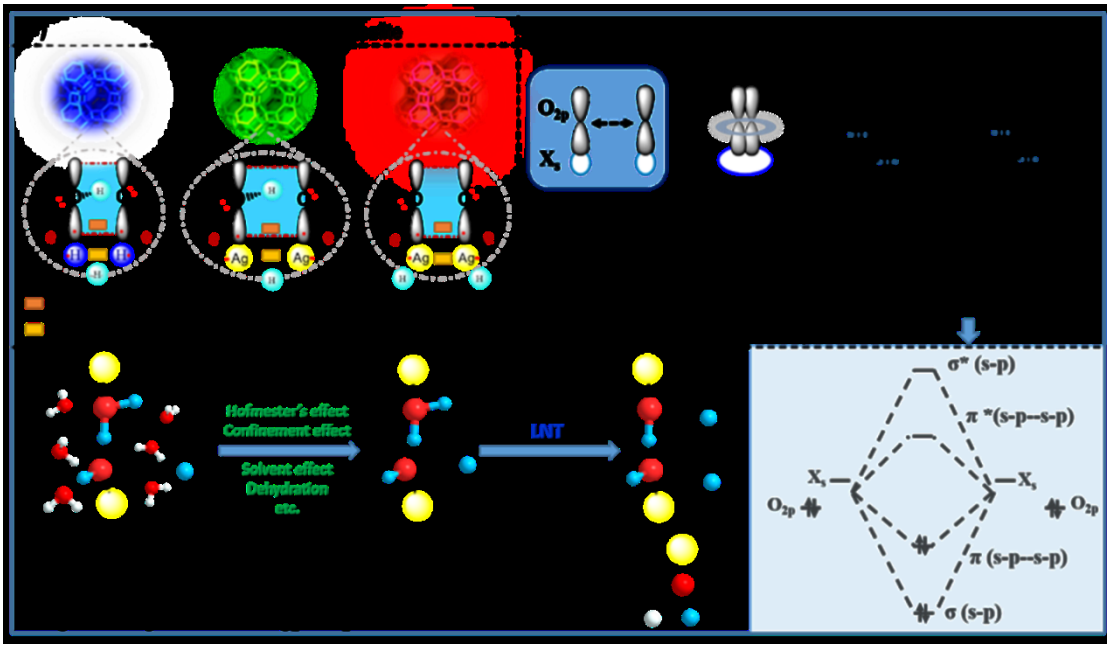

Figure 5. Schematic illustration of the interfacial orbital redistribution though space interactions induced bright and wavelength adjustable photoluminescence of Ag@LTA and corresponding energy level structure derived from molecular orbital theory.

Since single water molecule has not conjugated chromophore structure and /or even auxochromous group (Fig. 5a), water is intrinsically colorless liquid. Obviously, the physical origin of transient states mediating the absorption and PL (Fig. 2, Fig. 3, Fig. 4a and 4b) can't be simply explained by classical local excitation (spin-1 excitation) from eqa. 1 (ground state) to eqa. 2 (excited state) with a spin flip. However, if a singly hydrous hydroxide complex (or water-OH^- pair) is confined at nanoscale interface, multiple sets of transient species or states are feasible to produced due to the p orbital overlapping of oxygen atoms in varied x, y and z orbital directions (Fig. 5a) though space interactions.[13,27] In the chemical picture, using molecular orbital theory, the formation of transient states could be a result of relinear combination of extended sp hybrid orbitals between O p orbital and X s orbital (X could be Ag^+ ions, alkali metal ions, and protons) by space interactions (Fig. 5b). These new formed states are completely different from the covalent bonds, having the dynamic feature. In other way, we can image that, triggered by a strong vibration excitation process, such as photo-irradiation, a local high-energy sp hybrid state is ultrafast switched to two excited states with relative low energy levels, corresponding to the ultra-fast dynamics of TA (Fig. 4), i.e. in an extremely short time scale, at heterogeneous nano-interface, if water-metal (Ag^+) interaction involved, two antibonding orbitals with π and σ character are concurrently produced, respectively.

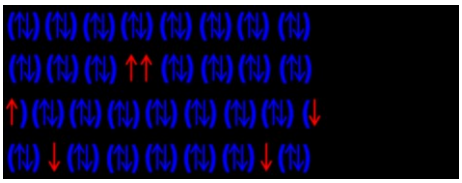

Figure 6. Schematic illustration of topological excitation process of hydrous hydroxide complex ($OH^{-}\cdot H_2O$).

Within the physical picture, the unique formation process and nature of the observed transient species or states fully verifies the topological excitation characteristics of multi-body quantum delocalization systems.[6-9] Here we just consider the simplest singly hydrous hydroxide complex ($OH^{-}\cdot H_2O$) as a many-body quantum system with two oxygen nucleus and 3 hydrogen nucleus and together 16 electrons (Fig. 6). According to 1D Ising model,[6,7] the ground state (GS) of 16 electrons could be consider as 8 spin-dimmer states formed by spin-singlets with local bond character (eqa. 1 in the ground state). By an operation of translation symmetry (eqa. 3 or 4 in the excited state), two spin 1/2 excitation (spinon) will be produced at the same time, it is also called topological excitation (domain wall).This system looks very simple, but, in fact, due to anisotropy of four pairs of electrons around each oxygen atom and proton transfer (PT) or shuttling, it is very complex system. In theory, at least, if the excitation energy is higher enough and the detection time is short enough, 6 transient species or states of ($OH^{-}\cdot H_2O$) with symmetrical H-bond should be captured on the TA spectra, in well agreement with the characteristic of multiple set of absorption on UV-visible spectrum (Fig. S2). But on TA spectrum (Fig. 4, c and e), only 3 transient species and states with π orbital character are observed with longer decay time, probably σ type transient states with the ultra-fast dynamic are not observed beyond the time resolution of our measurement. Aside of the microenvironment, the controlled experiments of the deuterium isotope effect and ultra-long second lifetime at LNT with bright green color clearly indicate that the energies and CT of multiple sets of absorption, emission bands and transient state the optical are strongly dependent on the PT process. Taken all together, singly hydrous hydroxide complex confined in nanospaces exhibit the typical feature of topological excitation dominated by MBQL mechanics.

Topological excitation induced transient species or states (Q_n) not only clearly answer the physical origin of abnormal PL emission features of non-conventional chromophores in the introduction section, more importantly, but also provide a completely new understanding on the kinetic of heterogeneous catalysis at confined nanoscale interface or space. These dynamic transient states, also so called the p band intermediate states (PBIS) previously reported by some of us,[13] herein we rename it the p band as a basic descriptor to describe of chemical reactivity because of the overlapping of p orbitals though space interaction. In order to describe the effect of p band

descriptor on the catalytic activity, we introduce a new interface orbital hybridized strength parameter ($IOHS_{M, MI, I}$) underlying the space interactions between surface molecules (denoted as M in the subscripts of IOHS), molecule-interface (denoted as MI) and even interfacial atoms (denoted as I) by space overlapping of atomic orbitals (AOs), to unveil the “black box” effect of classical heterogeneous catalysis.[31-34]

Since AOs are normalized according to the basic postulate of quantum mechanics and here topological excitation follows the many-body quantum delocalization mechanics, we deduce $IOHS_{MI} = IOHS_{MM} + IOHS_{I} = 1$, and two factors of $IOHS_{MM}$ and $IOHS_{I}$ are strongly competitive at nanoscale interface. If just considering the catalyst itself, the nature of active sites (or interfacial bond) of heterogeneous catalysts, is a dynamic redistribution of atomic orbitals, like the endless harmonic motion of the pendulum,[33] which is probably related to the peculiar nature of the Landau quantization of topological insulators, i.e., quantum oscillations.[35] Recently, a ligand-induced cooperative orbital redistribution dominating nanoscale molecule−surface interactions on the one-unit-thin TiO_2 Nanosheets was also observed.[36] In current Ag^{+}@LTA catalyst, we assume the confined surface states of $IOHS_{MI}$ correspond to chemisorption between the water O atom and Ag ions, then $IOHS_{O\text{-}Ag}$ is a descriptor measuring surface reactivity and the strength of chemisorption, while $IOHS_{MM}$ and $IOHS_{I}$ represent the contribution to adsorbate interaction between water and hydroxide ($IOHS_{MM} = IOHS_{O\text{-}O}$) though space interaction and metallophilic interactions between the metal ions ($IOHS_{I} = IOHS_{Ag\text{-}Ag}$), [37-40] respectively. If the reactants involve the formation process of p band, three positive effect to enhance chemical reactivity will take place: (1) the reaction barrier will significantly decreased due to the formation of multiple sets of transient states, which provide more reaction pathway to promote the electron transfer, i.e. the enhancement of catalytic activity or conversion; (2) the customer-tailored catalysts with designed active site will significantly enhance the selectivity of product by strengthening the interaction of reactant with $IOHS_{MM}$ by the maximum overlapping of the interacted orbitals with the same symmetry, e.g. selective hydrogenation of carbonyl groups interacted with surface hydroxide groups selectively; (3) Most importantly, the bond strength of reactant, reaction intermediate and product could be precisely tuned by the interplaying with IOHS factors, which is a quantitative implementation of the classical Sabatier principle defining the best catalyst for a given reaction in an optimum “bond strength”.[41]

In fact, currently thermally activated Ag@LTA zeolite is an ideal catalyst for the selective reduction of CO_2 to C_1 and C_2+ products at mild reaction conditions. As shown by in-situ DRIFTS at varied temperatures from 40^{o}C to 500^{o}C (Fig. 3e and Fig. 7), some typical C_1 and C_2 species, such as *C=O (~1960, ~2090 and ~2200 cm^{-1}),*HC=O (~1720 cm^{-1}), *O=CC=O (two separated bands of 1515 and 1586 cm^{-1} with indistinctive band center at 1560 cm^{-1}) and *OCCOH (1450 and 1415 cm^{-1}) species with typical fingerprint

stretching bands are observed at temperature less than 160 °C (Fig. 7).[42] Obviously, with further increase of measured temperature, these intermediate species were gradually eclipsed owing to the diffusive desorption of C_1, C_{2+} and non-activated CO_2 species. In addition, we found that all these fingerprint stretching bands exhibits the very broad breathing characteristic, implying the intrinsic dynamic feature of these transient species.

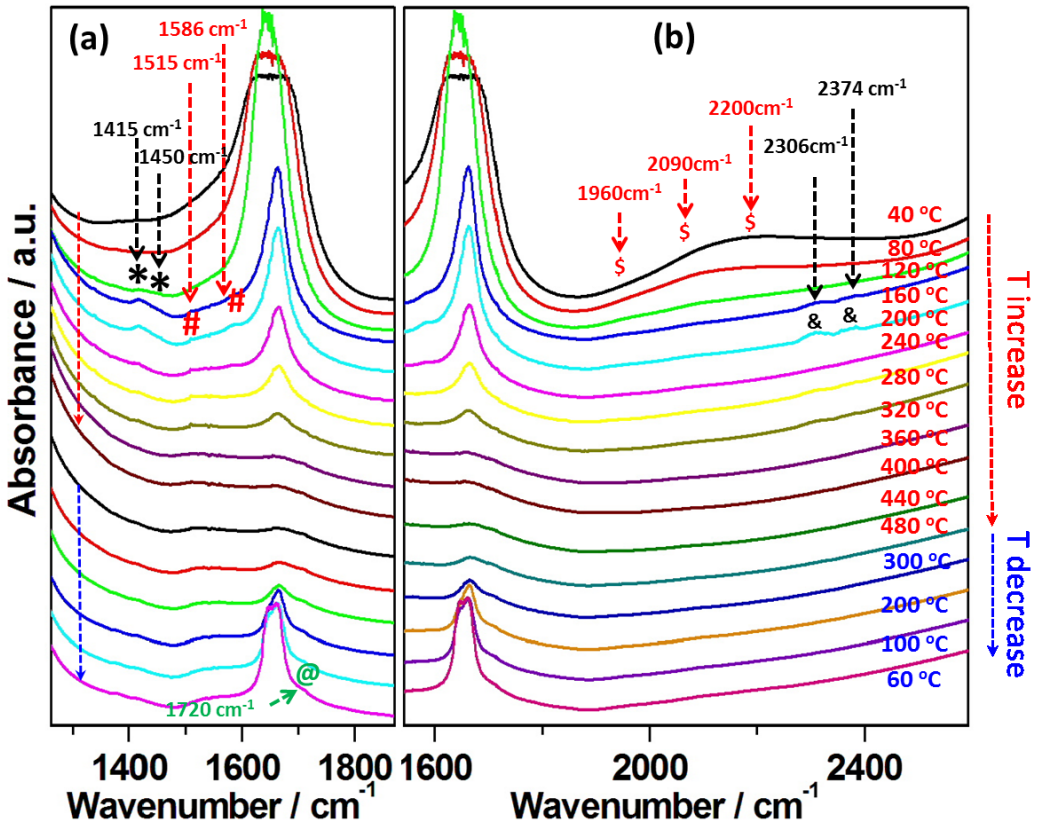

Figure 7. DRIFTS spectra of thermally activated Ag@LTA at varied temperatures in the region of 1300−1800 cm^{-1} (a) and 1600−2400 cm^{-1} (b).

Using our conceptual p band model with IOHS as descriptor, all the bonding or non-bonding electron pairs of O and C atoms involving many-body quantum localization could be regard as Fig. 8c). By precisely tailoring the interactions between the interface p band state of hydrous hydroxide complex and p orbitals of O and C atoms in CO_2 molecule, the selective reduction products of C_1 and C_{2+} and their corresponding reaction kinetics can be easily predicted (Fig. 8 a and 8b). For C_1 pathway, the reaction is initiated by a nucleophilic attacking of adsorbed basic hydroxide groups to C atom of CO_2 with positive charges, and the proton transfer is the rate-determining steps (RDS) for the final production of C_1, such as CO, CH_4 and CH_3OH (Fig. 8a). However, for C_{2+} product, the formation of key intermediates of *OCCHO or *OCCOH arising from the alternative coupling or dimerization between CO and/or hydrogenated CO (*CHO or *COH). *OCCO is a key step to trigger the C_{2+} route (Fig. 8b). From macro perspective, the delicate change of micro-environment surrounding the active sites determines the selectivity of final products. On the microscopic level, owing to the anisotropy (or polarity) of bonding and

non-bonding electron pairs (singlet dimmer) of interfacial O and C atoms in 2D spin liquid (Fig. 8c), the competitive space interaction of IOHS parameters dominates the final products, e.g., the selective conversion of CO_2 to ethylene and ethanol (Fig. 8c). [43-45] This model probably also answers the activation process of water molecules involved by electrocatalysis or optical catalysis, such as water splitting and the green synthesis of H_2O_2 at unique heterogeneous interface.[46-49] Thus, the mysterious internal force origin of catalysis is stemmed from the space interactions of atomic orbitals dominated by MBQL effect, which produce an ensemble of transient surface states with coupled spin and momentum quantum numbers. Owing to the preservation of time-reversal symmetry, this coupling protects the wave functions against disorder. These transient states have identical features of surface state of topological insulators.[13,32,35]

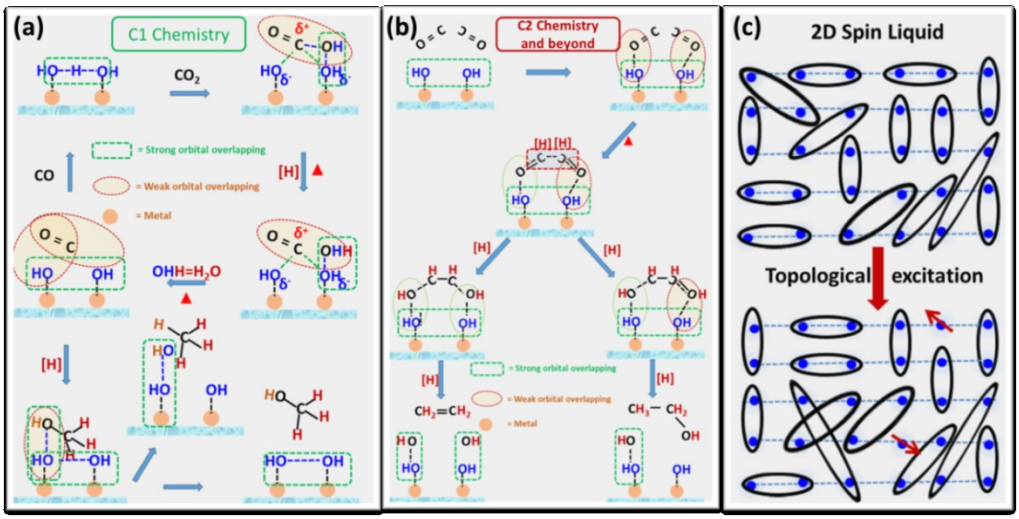

Figure 8. (a) Dynamic interface state regulated selective thermochemical CO_2 reduction to C_1 (a) and C_{2+} products (b) based on the conceptual p band model. (c) 2D spin liquid model dominated by many-body quantum localization (MBQL) at confined nanoscale interface.

Conclusions

In summary, we provided the direct evidence that intrinsically colorless water molecules could be a bright color emitter when they are confined at nanoscale interface or nanospace in the form of singly hydrous hydroxide complex. The ultra-fast Fs-TA technique, combined with the characterizations by steady optical absorption and fluorescent spectrum, we demonstrated that the physical origin of PL emission of water molecules is originated from the topological excitation dominated by many-body quantum delocalization mechanics, instead of conventional local excitation mechanics. The energy and quantum efficiency of PL emission are extremely sensitive to the confined microenvironments dominated by H-bond interactions. The proposed conceptual p band model is not only limited to water molecules containing O atoms at heterogeneous nanoscale interface, but also plausible to other

ligands containing other heteroatoms with p orbital contribution, such as O, N, C, S, P etc. Most importantly, the proposed IOHS descriptor provides a completely new understanding on the micro-kinetic of heterogeneous catalysis on the atomic orbital level.

Author Contributions: TQY and XDH equally contribute to this research. KZ conceived and directed the project. KZ and TQY analyzed all the data and co-designed the figures. KZ wrote the manuscript with the help of TQY. TQY performed the PL and TA measurements. XDH synthesized the materials. BQS and BP performed the SEM and TEM measurements. All authors have read and agreed to the published version of the manuscript.

Acknowledgments: This research was funded by the NSFC (21872053 and 21573074), the Science and Technology Commission of Shanghai Municipality (19520711400), the CAS key laboratory of Low-Coal Conversion Science & Engineering (KLLCCSE-201702), and the JORISS program, the Postdoctoral Science Foundation of China (2018M640360). K.Z. thanks ENS de Lyon for a temporary position as an invited professor in France.

Reference

1 Yang, T.-Q., Bo-Peng, Zhou, J.-F., Shan, B.-Q. & Zhang, K. Hydrogen-Bonded Water Clusters Confined in Nanocavity as Bright Color Emitters. *ChemRxiv*, doi:10.26434/chemrxiv.12927452 (2020).

2 EWLES, J. Water as an Activator of Luminescence. *Nature* **125**, 706-707 (1930).

3 Grandjean, D. *et al.* Origin of the bright photoluminescence of few-atom silver clusters confined in LTA zeolites. *Science* **361**, 686–690 (2018).

4 Horwlstrnr, A. l. M. & Rossurc'N, G. R. A spectroscopic study of irradiation colodlg _of amazonite: structurally hydrous, Pbbearing feldsPar. *Amefican Mineralogis* **70**, 794-780 (1985).

5 Garcia-Guinea, J., Correcher, V., Can, N., Garrido, F. & Townsend, P. D. Cathodoluminescence spectra recorded from surfaces of solids with hydrous molecules. *J. Electron. Spectrosc. Relat. Phenom.* **227**, 1-8, doi:10.1016/j.elspec.2018.05.008 (2018).

6 Levin, M. A. & Wen, X.-G. String-net condensation: A physical mechanism for topological phases. *Phys. Rev. B* **71**, 045110, doi:10.1103/PhysRevB.71.045110 (2005).

7 Chen, X., Gu, Z.-C. & Wen, X.-G. Classification of gapped symmetric phases in one-dimensional spin systems. *Phys. Rev. B* **83**, 035107, doi:10.1103/PhysRevB.83.035107 (2011).

8 Chen, X., Gu, Z.-C., Liu, Z.-X. & Wen, X.-G. Symmetry protected topological orders and the group cohomology of their symmetry group. *Phys. Rev. B* **87**, 155114, doi:10.1103/PhysRevB.87.155114 (2013).

9 Savary, L. & Balents, L. Quantum spin liquids: a review. *Rep. Prog. Phys.* **80**, 016502, doi:10.1088/0034-4885/80/1/016502 (2017).

10 Chen, Y. *et al.* Photoemission mechanism of water-soluble silver nanoclusters: ligand-to-metal-metal charge transfer vs strong coupling between surface plasmon and emitters. *Journal of the American Chemical Society* **136**, 1686-1689, doi:10.1021/ja407911b (2014).

11 Yang, T. *et al.* Interfacial Clustering-Triggered Fluorescence-Phosphorescence Dual Solvoluminescence of Metal Nanoclusters. *J. Phys. Chem. Lett.* **8**, 3980-3985,

doi:10.1021/acs.jpclett.7b01736 (2017).

12 Yang, T. Q. *et al.* Origin of the Photoluminescence of Metal Nanoclusters: From Metal-Centered Emission to Ligand-Centered Emission. *Nanomaterials (Basel)* **10**, doi:10.3390/nano10020261 (2020).

13 Yang, T. *et al.* P band intermediate state (PBIS) tailors photoluminescence emission at confined nanoscale interface. *Commun. Chem.* **2**, doi:10.1038/s42004-019-0233-1 (2019).

14 Crespo-Hernandez, C. E., Cohen, B. & Kohler, B. Base stacking controls excited-state dynamics in A.T DNA. *Nature* **436**, 1141-1144, doi:10.1038/nature03933 (2005).

15 Markovitsi, D. UV-induced DNA Damage: The Role of Electronic Excited States. *Photochem Photobiol* **92**, 45-51, doi:10.1111/php.12533 (2016).

16 Zhang, Y., de La Harpe, K., Beckstead, A. A., Improta, R. & Kohler, B. UV-Induced Proton Transfer between DNA Strands. *J. Am. Chem. Soc.* **137**, 7059-7062, doi:10.1021/jacs.5b03914 (2015).

17 Zhou, Q. *et al.* Clustering-Triggered Emission of Nonconjugated Polyacrylonitrile. *Small* **12**, 6586-6592, doi:10.1002/smll.201601545 (2016).

18 Yuan, W. *et al.* Visualizing H2O molecules reacting at TiO2 active sites with transmission electron microscopy. *Science* **367**, 428–430 (2020).

19 Borodin, D. *et al.* Following the microscopic pathway to adsorption through chemisorption and physisorption wells. *Science* **369**, 1461–1465 (2020).

20 Fenwick, O. *et al.* Tuning the energetics and tailoring the optical properties of silver clusters confined in zeolites. *Nat. Mater.* **15**, 1017-1022, doi:10.1038/nmat4652 (2016).

21 Seifert, R., Kunzmann, A. & Calzaferri, G. The Yellow Color of Silver-Containing Zeolite A. *Angew. Chem. Int. Ed.* **37**, 1522-1524 (1998).

22 Coutino-Gonzalez, E. *et al.* Silver Clusters in Zeolites: From Self-Assembly to Ground-Breaking Luminescent Properties. *Acc. Chem. Res.* **50**, 2353-2361, doi:10.1021/acs.accounts.7b00295 (2017).

23 Coutino-Gonzalez, E. *et al.* Thermally activated LTA(Li)–Ag zeolites with water-responsive photoluminescence properties. *J. Mater. Chem. C* **3**, 11857-11867, doi:10.1039/c5tc02723c (2015).

24 Lin, H., Imakita, K. & Fujii, M. Reversible emission evolution from Ag activated zeolite Na-A upon dehydration/hydration. *Appl. Phys. Lett.* **105**, doi:10.1063/1.4902530 (2014).

25 Zhang, K. *et al.* Mononuclear-dinuclear equilibrium of grafted copper complexes confined in the nanochannels of MCM-41 silica. *Chem. Eur. J.* **17**, 14258-14266, doi:10.1002/chem.201102026 (2011).

26 Holmlid, L. The diffuse interstellar band carriers in interstellar space: all intense bands calculated from He doubly excited states embedded in Rydberg Matter. *Mon. Not. R. Astron. Soc.* **384**, 764-774, doi:10.1111/j.1365-2966.2007.12753.x (2008).

27 Hoffmann, R. Interaction of Orbitals through Space and through Bonds. *Acc. Chem. Res.* **4**, 1-9 (1971).

28 Hua, Y. *et al.* Cation Effect on the Electronic Excited States of Guanine Nanostructures Studied by Time-Resolved Fluorescence Spectroscopy. *J. Phys. Chem. C* **116**, 14682-14689, doi:10.1021/jp303651e (2012).

29 Miannay, F. o.-A., Banyasz, A., Gustavsson, T. & Markovitsi, D. Excited States and Energy Transfer in G-Quadruplexes. *J. Phys. Chem. C* **113**, 11760–11765 (2009).

30 Ma, C., Chan, R. C., Chan, C. T., Wong, A. K. & Kwok, W. M. Real-time Monitoring Excitation Dynamics of Human Telomeric Guanine Quadruplexes: Effect of Folding Topology, Metal Cation, and Confinement by Nanocavity Water Pool. *J. Phys. Chem. Lett.* **10**, 7577-7585, doi:10.1021/acs.jpclett.9b02932 (2019).

31 Park, J. Y., Baker, L. R. & Somorjai, G. A. Role of Hot Electrons and Metal–Oxide Interfaces in Surface Chemistry and Catalytic Reactions. *Chem. Rev.* **115**, 2781-2817, doi:10.1021/cr400311p (2015).

32 Lindström, B. & Pettersson, L. J. A Brief History of Catalysis. *CATTECH* **7**, 130-138, doi:10.1023/A:1025001809516 (2003).

33 Yang, F., Deng, D., Pan, X., Fu, Q. & Bao, X. Understanding nano effects in catalysis. *Natl. Sci. Rev.* **2**, 183-201, doi:10.1093/nsr/nwv024 (2015).

34 Norskov, J. K. *et al.* The nature of the active site in heterogeneous metal catalysis. *Chem. Soc. Rev.* **37**, 2163-2171, doi:10.1039/b800260f (2008).

35 Analytis, J. G. *et al.* Two-dimensional surface state in the quantum limit of a topological insulator. *Nat. Phys.* **6**, 960-964, doi:10.1038/nphys1861 (2010).

36 Xiang, G. *et al.* Probing Ligand-Induced Cooperative Orbital Redistribution That Dominates Nanoscale Molecule-Surface Interactions with One-Unit-Thin TiO2 Nanosheets. *Nano Lett.* **18**, 7809-7815, doi:10.1021/acs.nanolett.8b03572 (2018).

37 Yam, V. W., Au, V. K. & Leung, S. Y. Light-Emitting Self-Assembled Materials Based on d(8) and d(10) Transition Metal Complexes. *Chem. Rev.* **115**, 7589-7728, doi:10.1021/acs.chemrev.5b00074 (2015).

38 Pyykko, P. & Mendizabal, F. Theory of the d10 -d1 Closed-Shell Attraction: 2. Long-Distance Behaviour and Nonadditive Effects in Dimers and Trimers of Type [(X-Au-L),] (n = 2, 3; X = Cl, I, H; L = PH,, PMe,, -N=CH). *Chem. Eur. J.* **3**, 1458-1465 (1997).

39 Schmidbaur, H. The Aurophilicity Phenomenon: A Decade of Experimental Findings, Theoretical Concepts and Emerging Applications. *Gold Bulletin* **33**, 3-10 (2000).

40 Schmidbaur, H. & Schier, A. A briefing on aurophilicity. *Chem. Soc. Rev.* **37**, 1931-1951, doi:10.1039/b708845k (2008).

41 Medford, A. J. *et al.* From the Sabatier principle to a predictive theory of transition-metal heterogeneous catalysis. *J. Catal.* **328**, 36-42, doi:10.1016/j.jcat.2014.12.033 (2015).

42 Kim, Y. *et al.* Time-resolved observation of C–C coupling intermediates on Cu electrodes for selective electrochemical CO2 reduction. *Energy Environ. Sci.*, doi:10.1039/d0ee01690j (2020).

43 Tackett, B. M., Gomez, E. & Chen, J. G. Net reduction of CO2 via its thermocatalytic and electrocatalytic transformation reactions in standard and hybrid processes. *Nat. Catal.* **2**, 381-386, doi:10.1038/s41929-019-0266-y (2019).

44 Handoko, A. D., Wei, F., Jenndy, Yeo, B. S. & Seh, Z. W. Understanding heterogeneous electrocatalytic carbon dioxide reduction through operando techniques. *Nature Catalysis* **1**, 922-934, doi:10.1038/s41929-018-0182-6 (2018).

45 Birdja, Y. Y. *et al.* Advances and challenges in understanding the electrocatalytic conversion of carbon dioxide to fuels. *Nat. Energy* **4**, 732-745, doi:10.1038/s41560-019-0450-y (2019).

46 Grimaud, A. *et al.* Activating lattice oxygen redox reactions in metal oxides to catalyse oxygen evolution. *Nat. Chem.* **9**, 457-465, doi:10.1038/nchem.2695 (2017).

47 Hong, W. T. *et al.* Toward the rational design of non-precious transition metal oxides for

oxygen electrocatalysis. *Energy & Environ. Sci.* **8**, 1404-1427, doi:10.1039/c4ee03869j (2015).

48 Lee, J. K. *et al.* Spontaneous generation of hydrogen peroxide from aqueous microdroplets. *Proc. Natl. Acad. Sci. U.S.A* **116**, 19294-19298, doi:10.1073/pnas.1911883116 (2019).

49 Lee, J. K., Samanta, D., Nam, H. G. & Zare, R. N. Micrometer-Sized Water Droplets Induce Spontaneous Reduction. *J. Am. Chem. Soc.* **141**, 10585-10589, doi:10.1021/jacs.9b03227 (2019).

Topological excitation of singly hydrated hydroxide complex in confined sub-nanospace for bright color emission and heterogeneous catalysis

Xiao-Dan Hu,[1] Tai-Qun Yang,[1] Bing-Qian Shan,[1] Bo Peng,[1] Kun Zhang[1,2,3]*

[1] Shanghai Key Laboratory of Green Chemistry and Chemical Processes, Laboratory of Interface and Water Science, College of Chemistry and Molecular Engineering, East China Normal University, Shanghai 200062, China;

[2] Laboratoire de chimie, Ecole Normale Supérieure de Lyon, Institut de Chimie de Lyon, Université de Lyon, 46 Allée d'italie, 69364 Lyon cedex 07, France;

[3] Shandong Provincial Key Laboratory of Chemical Energy Storage and Novel Cell Technology, School of Chemistry and Chemical Engineering, Liaocheng University, Liaocheng, 252059, Shandong, P. R. China.

* Correspondence: kzhang@chem.ecnu.edu.cn (K.Z.)

Experimental Section

Chemicals

All chemical reagents were directly used without any isolation or purification. LTA zeolite (Na-LTA, Si/Al=1~2) and Y-type zeolite (Si/Al=2~3) were ordered from Nankai University Catalyst Co., Ltd.. $AgNO_3$ Polyacrylic acid (PAA) were ordered from Sigma-Aldrich. NaOH, HNO_3 and all the other organic solvents were purchased from Sinopharm Chemicals Beijing Co. Beijing, China. Ultrapure water with a resistivity of 18.2 MΩ·cm was used throughout all experiments.

Synthesis

Synthesis of Ag loaded zeolite (Ag-LTA)

The silver loaded zeolite Ag-LTA(Na) was prepared by suspending 1 gram of the zeolite material (Na-LTA, Si/Al = 1~2) in 500 mL of a silver nitrate aqueous solution, the suspension was then agitated for 2 hours in the dark. The powder was recovered by filtration using a Büchner filter and washed several times with milliQ water. Then the sample was calcined overnight at 450 °C (5 °C min^{-1}) following 2 steps of 15 minutes each at 100 and 150 °C to prevent any damage in the zeolite structure during the calcination process. After heat treatment the sample was cooled under ambient conditions, allowing the sample to reach a fully hydrated state, and stored in the dark for further analysis.

Synthesis of PAA-Ag NCs:

The synthesis of luminescent PAA-Ag NCs refers to literature reports.[1] Typically, The PAA (0.4 M, 20 mL) were dissolved in an aqueous solution of 0.5 g sodium hydroxide, then the mixture was added into the freshly prepared aqueous solutions of $AgNO_3$ (0.1 M, 20 mL) under gentle stirring (600 rpm) at room temperature. NaOH or 0.1 M HNO3 adjusted the pH. After 10 min, the solution was transferred into fluorescence cuvettes, followed by the UV irradiation (photoreduction) at λ=365 nm (Shanghai Jihui Scientific Analyze Instrument Co., China, ZF-20D, 24W) at various time intervals. The silver nanoclusters have good stability at low temperature and were stored at 4 °C.

Characterization

Absorption (or extinction) spectra were collected with a two-beam UV-Vis spectrometer (PERSEE TU-1901, China). DRIFTS measurement: Catalyst samples were packed into a Harrick Praying Mantis high temperature reaction chamber (ZnSe windows) mounted inside of a Thermo Scientific Praying Mantis diffuse reflectance adapter, set inside of a Thermo Scientific Nicolet iS10 FT-IR spectrometer. N_2 were flowed to the reaction chamber using Teledyne mass flow controllers. Thermogravimetric analysis (TGA) was conducted on a NETZSCH STA449F3 analyzer under air atmosphere (flow rate of 50 mL·min−1). The X-ray diffraction (XRD) patterns were required using a Rigaku Ultima Discover X-Ray Diffractometer at a wavelength of Cu Kα (1.5405 Å). The SEM images were taken using Hitachi S-4800 microscope. HR-TEM images of NCs were collected with a JEOL JEM 2010 microscope operating at 200 kV. Fluorescence was measured by using a FluorMax-4 fluorimeter (Horiba, Japan). Fluorescence lifetime was measured with a homebuilt time-correlated single photon counting (TCSPC) system with a time resolution of sub-100 ps. Phosphorescence lifetime was excited with a μF2 lamp and measured with FLS 980 spectrofluorimeter (Edinburgh Instruments). The transient absorption (TA) measurements were conducted in a femtosecond transient absorption spectrometer (Helios Fire, Ultrafast System) with pump probe beams generated with a Ti:sapphire laser system (Astrella, 800 nm, 100 fs, 7 mJ/pulse, and 1 kHz repetition rate, Coherent Inc.). A fraction of the fundamental beam was focused into the sapphire to generate a white light continuum probe beam from 420 to 800 nm. Another fraction of the fundamental beam was used to produce pump beams via an optical parametric amplifier (OPerA Solo, Coherent Inc.), and the power was adjusted to ~0.3 mW by a neutral-density filter wheel. All experiments were carried out at room temperature. 2 mm cuvettes were used for all spectroscopy measurements.

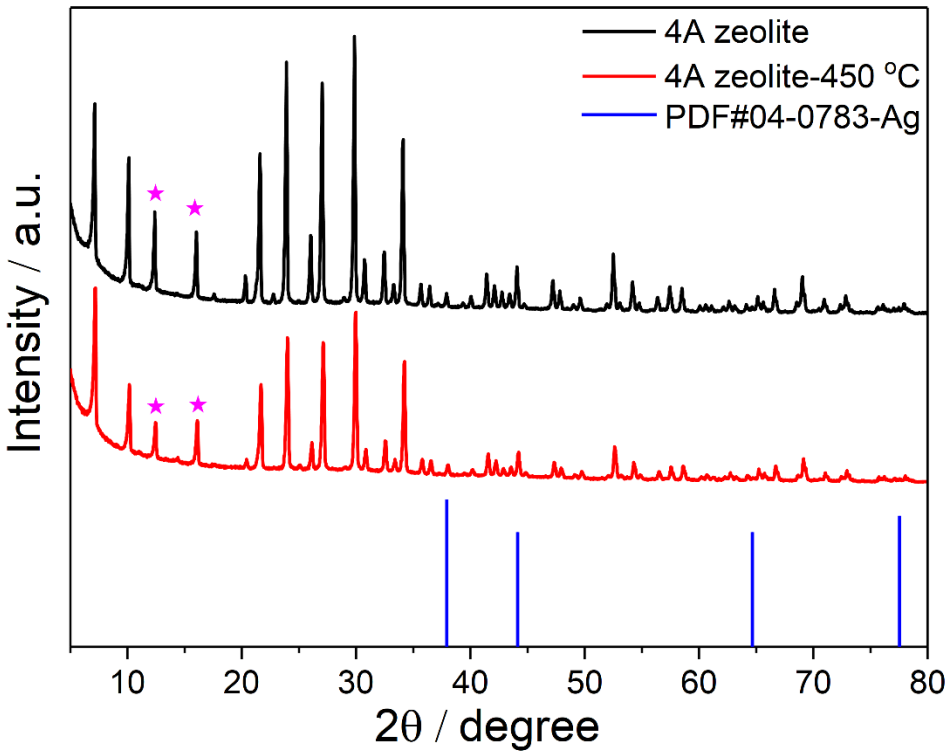

Figure S1. XRD patterns of 4A zeolite and Ag@LTA-450 °C.

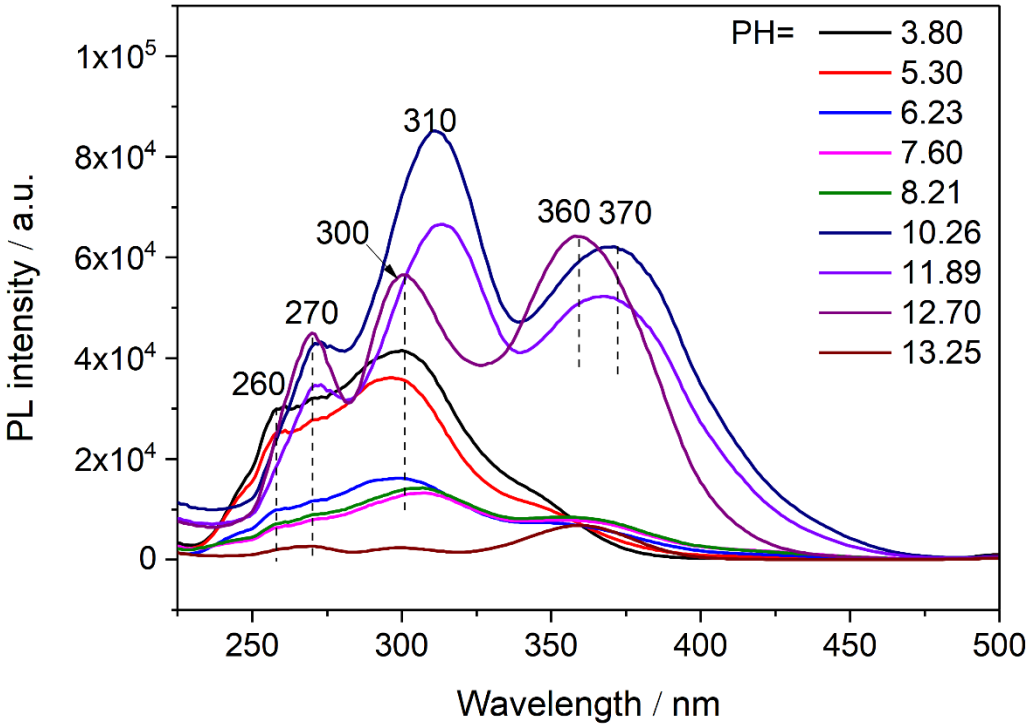

Figure S2. Excitation spectra of Ag@LTA-450 °C solution at different pH condition.

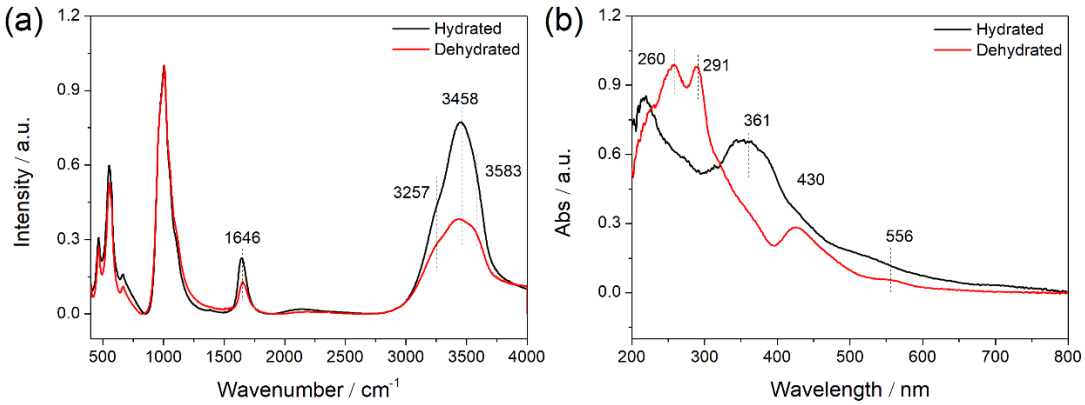

Figure S3. FTIR spectra (a) and UV-Vis absorption spectra (b) of hydrated Ag@LTA-450 ^{o}C under hydrated and dehydrated state.

Table S1. XPS peak parameters for the O (Fig. 1g) and Ag (Fig. 1h) states of Ag@LTA-450 ^{o}C.

Atom	Item	binding energy	content
O_{1s}	Ag^{+}-OH^{-}	530.6 eV	16.4%
	Ag^{+}-H_2O	531.7 eV	17.8%
	Si-O-Si	532.8 eV	65.8%
Ag_{3d}	Ag^{+}	368.3 eV	56.5%
	Ag^{0}	370.1 eV	43.5%

Table S2. Lifetime parameters of Ag@LTA-450 ^{o}C in water and DMSO solution. The steady state optical characterizations are presented in Figure 2, b and e.

Item	α_1	α_2	α_2	τ_1	τ_2	τ_3	χ^2	Average lifetime
In water	33.4%	40.8%	25.8%	0.4ns	1.9ns	4.2ns	1.10	3.0ns
In DMSO	78.0%	22.0%	---	155.6μs	350.7μs	---	0.99	231.1μs

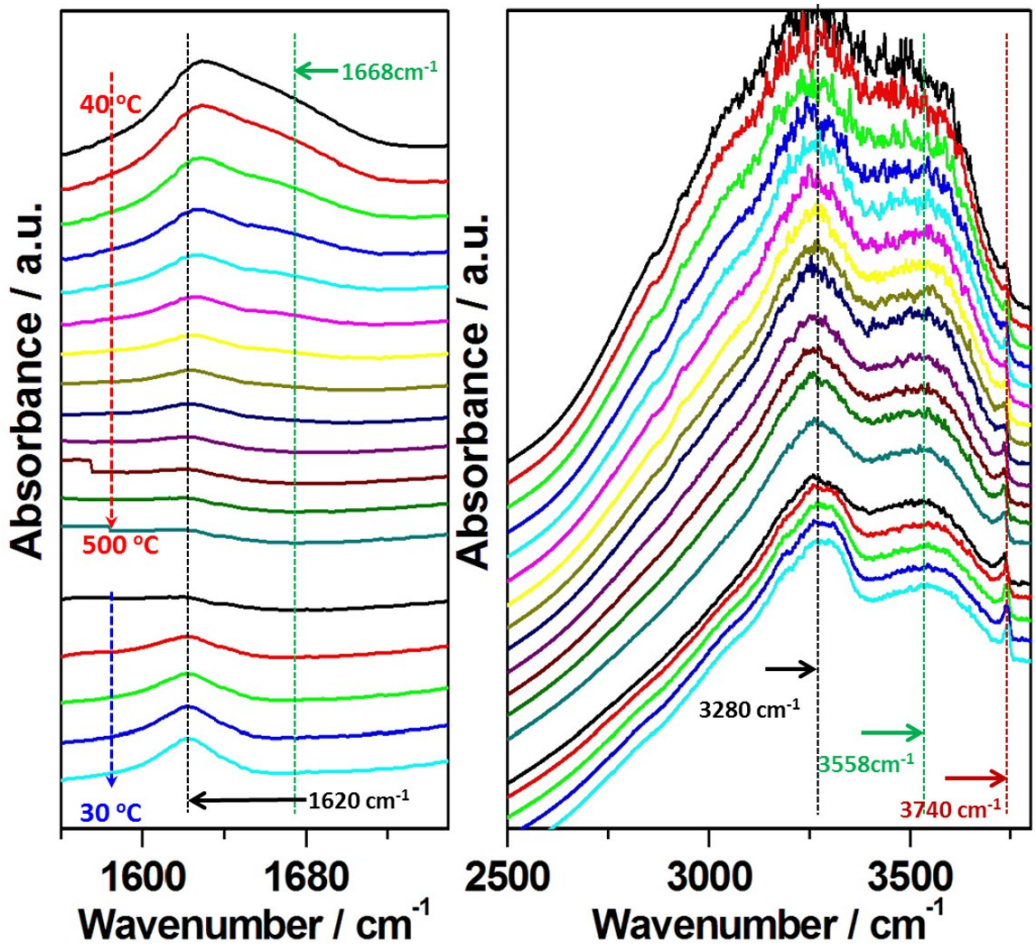

Figure S4. In situ DRIFTS of NH_4^+@LTA-500 ^oC during a programmed heating and cooling process.

Table S3. Lifetime parameters of NH_4^+-Y-type zeolite at room temperature (RT) and liquid nitrogen temperature (LNT). The steady state optical characterizations are presented in Figure 3e.

Item	α_1	α_2	τ_1	τ_2	χ^2	Average lifetime
In RT	97.4%	2.6%	1.58ns	5.29ns	1.10	3.0ns
In LNT	78.0%	22.0%	0.10s	0.94s	0.99	0.7s

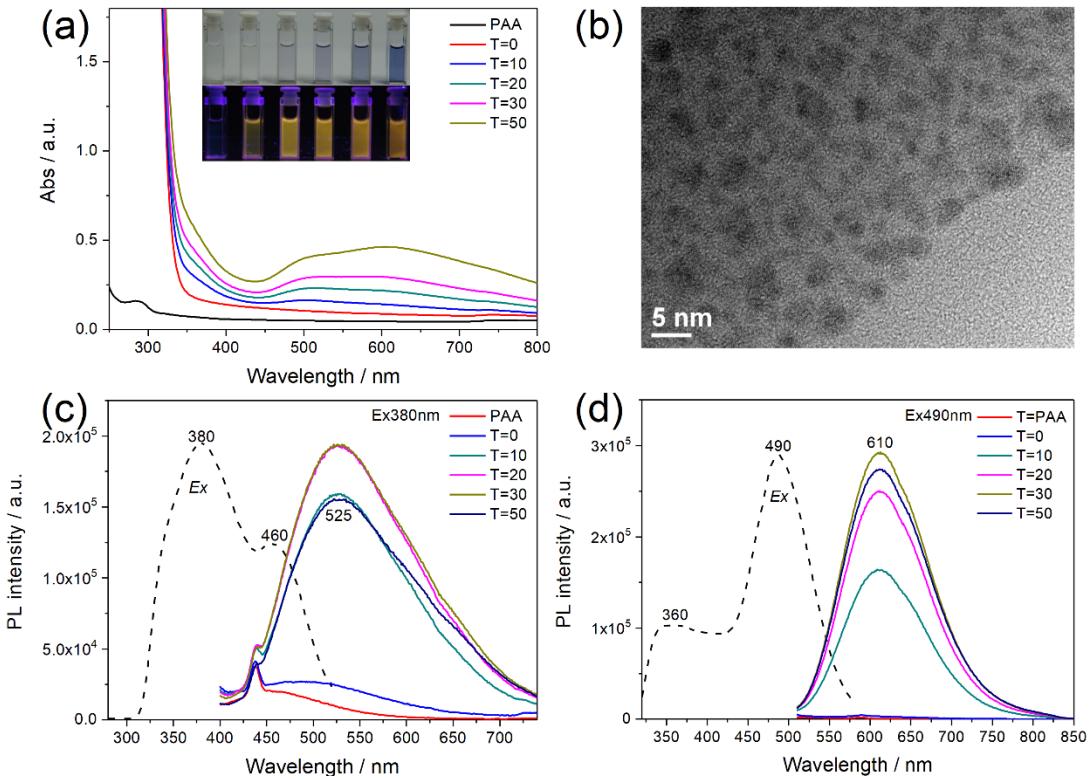

Figure S5. (a) UV−vis absorption of the freshly prepared PAA-Ag NCs at various radiation times. Corresponding PL spectra excited at 380 nm (c) and 490 nm (d). Inset images show the corresponding photographs of PAA-Ag NCs under room and UV light exposure at λ = 365 nm. (b) TEM image of freshly prepared PAA-Ag NC.

Table S4. Lifetime parameters of PAA-Ag NCs in water and DMSO solution. The steady state optical characterizations are presented in Figure 4, a and b.

Item	Em	α_1	α_2	α_3	τ_1	τ_2	τ_3	χ^2	Average lifetime
In water	610nm	5.2%	24.3%	70.5%	3.0ns	1.0 ns	0.1 ns	1.08	1.5ns
	460nm	1.1%	21.8%	77.2%	3.6ns	0.7 ns	0.2 ns	1.10	0.9ns
In DMSO	530nm	41.2%	58.8%	---	115.1 μs	32.8μs	---	0.98	91.3μs

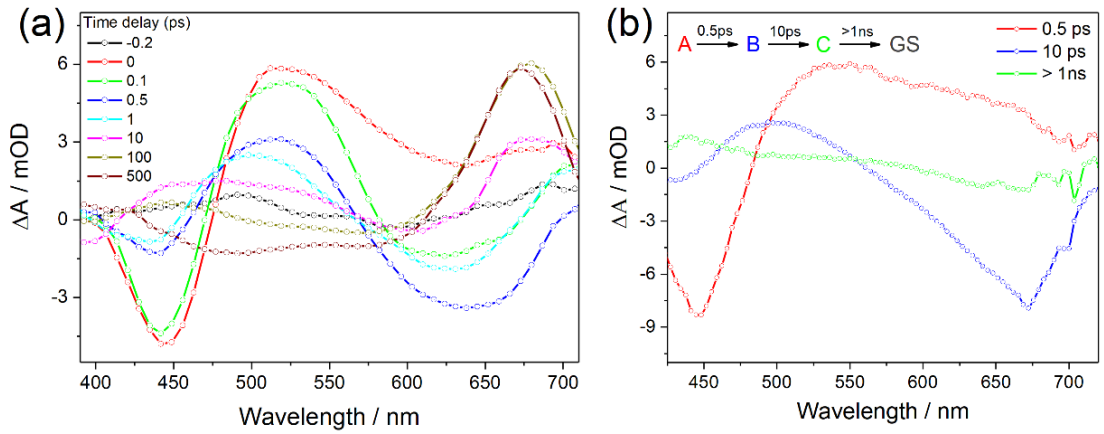

Figure S6. (a) Two-dimensional transient absorption spectra at selected time delays for PAA-Ag NCs in water solution. (b) Species-associated spectra obtained from global fitting on the TA data.

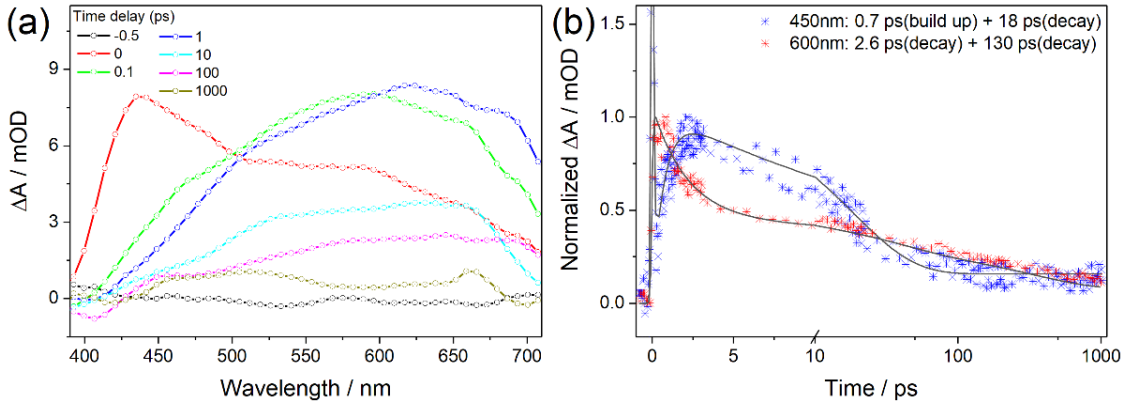

Figure S7. (a) Two-dimensional transient absorption spectra at selected time delays for PAA-Ag NCs in DMSO solution. (b) Selected decay traces and corresponding fitting, the fitting results are summarized in Table S4.

Table S5. Time constants of PAA-Ag NCs in water and DMSO solutions obtained using two components fitting. The fitting parameters was little different with global fitting results, since the global fitting need to take all wavelength-decay into consideration.

Item	probe	A_1	τ_1 (ps)	A_2	τ_2(ps)	offset
In water	443nm	-0.008	0.6	0.001	350	0
	520nm	0.005	0.7	0.002	14.5	-0.0004
	590nm	-0.002	3.0	0.003	10.3	-0.0005
	680nm	-0.002	13.7	---	---	---
In DMSO	450nm	-0.003	0.7	0.0025	18	0.0004
	550nm	0.0043	3.1	0.0024	115.6	0.0008
	600nm	0.0051	2.6	0.0026	137.6	0.0009
	650nm	0.0048	2.6	0.0023	150.6	0.0012

Reference

1. Chen, Y.; Yang, T.; Pan, H.; Yuan, Y.; Chen, L.; Liu, M.; Zhang, K.; Zhang, S.; Wu, P.; Xu, J., Photoemission mechanism of water-soluble silver nanoclusters: ligand-to-metal-metal charge transfer vs strong coupling between surface plasmon and emitters. *Journal of the American Chemical Society* **2014,** *136* (5), 1686-9.